Supplemental information: Cotunneling drag effect in Coulomb-coupled quantum dots

A. J. Keller,[1,*] J. S. Lim,[2] David Sánchez,[3] Rosa López,[3] S. Amasha,[1,†]
J. A. Katine,[4] Hadas Shtrikman,[5] and D. Goldhaber-Gordon[1,‡]

[1]*Department of Physics, Stanford University, Stanford, California 94305, USA*
[2]*School of Physics, Korea Institute for Advanced Study, Seoul 130-722, Korea*
[3]*IFISC (UIB-CSIC), E-07122 Palma de Mallorca, Spain*
[4]*HGST, San Jose, CA 95135, USA*
[5]*Department of Condensed Matter Physics, Weizmann Institute of Science, Rehovot 96100, Israel*

A. CAPACITANCES

To extract the capacitances in our device, we begin by assuming the usual electrostatic model for a double quantum dot (DQD) [1], which has a capacitor between each dot and its source and drain leads (C_{Si} and C_{Di}, for $i \in \{1,2\}$), each dot and its gate (C_{Pi}), and a capacitor between the dots (C_m). We define C_i to be the total capacitance of dot i, e.g. $C_1 = C_{P1} + C_{S1} + C_m +$ capacitances to ground.

The electrostatic energy of the system $\vec{Q} \cdot \vec{V}/2$ is given by:

$$\begin{aligned}\widetilde{U}(N_1,N_2) = &\frac{1}{2}U_1N_1^2 + \frac{1}{2}U_2N_2^2 + UN_1N_2 - \frac{1}{2|e|}\sum_{i\in\{1,2\}} U_i\left\{C_{Pi}V_{Pi}N_i + C_{Si}V_{Si}N_i\right\} \\ &- \frac{1}{2|e|}U\left\{C_{P1}V_{P1}N_2 + C_{P2}V_{P2}N_1 + C_{S1}V_{S1}N_2 + C_{S2}V_{S2}N_1\right\}\end{aligned} \tag{1}$$

where we let $Q_i = -|e|N_i$. The addition energies of the system are given by:

$$U_1 = e^2\frac{C_2}{C_1C_2 - C_m^2} = \frac{e^2}{C_1}X \tag{2}$$

$$U_2 = e^2\frac{C_1}{C_1C_2 - C_m^2} = \frac{e^2}{C_2}X \tag{3}$$

$$U = e^2\frac{C_m}{C_1C_2 - C_m^2} = \frac{e^2}{C_m}(X-1) \tag{4}$$

where

$$X = \frac{1}{\left(1 - \frac{C_m^2}{C_1C_2}\right)} \tag{5}$$

It follows that $C_m/C_2 = U/U_1$ and $C_m/C_1 = U/U_2$, so we may also write

$$X = \frac{1}{\left(1 - \frac{U^2}{U_1U_2}\right)} \tag{6}$$

The addition energies can may be extracted simply from transport measurements and we use the values reported in our previous work [2]. We obtain $X = 1.006$ in terms of the addition energies $U_1 = 1.2$ meV, $U_2 = 1.5$ meV, and $U = 0.1$ meV. We then obtain $C_1 = 130$ aF, $C_2 = 107$ aF, $C_m = 9.0$ aF.

The effective dot levels are given by:

$$\mu_1(N_1,N_2) = \widetilde{U}(N_1,N_2) - \widetilde{U}(N_1-1,N_2) \tag{7}$$

$$\mu_2(N_1,N_2) = \widetilde{U}(N_1,N_2) - \widetilde{U}(N_1,N_2-1) \tag{8}$$

The slopes of linear features seen in source-drain bias spectroscopy correspond to conditions on the effective dot levels. The slopes may be related to the capacitances. The slopes m_{i1} and m_{j1} in Supp. Fig. 1(a) are:

$$m_{i1} = -\frac{C_{P1}}{C_{S1}} \tag{9}$$

$$m_{j1} = \frac{C_{P1}}{2C_1/X - C_{S1}} \tag{10}$$

These can be used to solve for the remaining capacitances:

$$C_{P1} = \frac{2C_1}{X}\frac{m_{i1}m_{j1}}{m_{i1} - m_{j1}} \tag{11}$$

$$C_{S1} = -\frac{2C_1}{X}\frac{m_{j1}}{m_{i1} - m_{j1}} \tag{12}$$

The capacitances C_{P2} and C_{S2} are similarly related to the slopes m_{i2} and m_{j2} in Supp. Fig. 1(b). We find $C_{P1} = 17.5$ aF, $C_{S1} = 60.9$ aF, $C_{P2} = 11.9$ aF, $C_{S2} = 53.9$ aF.

At this point we can check for self-consistency using other measurements. Supplementary Figure 1(c) and Supp. Fig. 1(d) show part of the charge stability diagram (note the axes are swapped between (c) and (d)). In Supp. Fig. 1(c), the peak in G_1 corresponds to constant μ_1. The following condition holds:

$$U_1 C_{P1}\Delta V_{P1} + U C_{P2}\Delta V_{P2} = 0 \tag{13}$$

Therefore we would expect that the measured slope $m = \Delta V_{P1}/\Delta V_{P2} = -0.166$ should equal $-UC_{P2}/U_1C_{P1} = -0.0567$. The large discrepancy indicates that the typical electrostatic model of a DQD is insufficient to describe our data.

To account for the discrepancy we introduce direct capacitances between reservoir S1 and dot 2 ($C_{S1,2}$), and vice versa. We also introduce capacitances between gate P1 and dot 2 ($C_{P1,2}$), and vice versa, though these will be small. The total capacitances C_1 and C_2 will now include these extra capacitances. To Eqn. 1 we must add corresponding terms:

$$\begin{aligned} &-\frac{1}{2|e|}U_1\left\{C_{P2,1}N_1V_{P2} + C_{S2,1}N_1V_{S2}\right\} - \frac{1}{2|e|}U_2\left\{C_{P1,2}N_2V_{P1} + C_{S1,2}N_2V_{S1}\right\} \\ &-\frac{1}{2|e|}U\left\{C_{P1,2}N_1V_{P1} + C_{P2,1}N_2V_{P2} + C_{S1,2}N_1V_{S1} + C_{S2,1}N_2V_{S2}\right\} \end{aligned} \tag{14}$$

While the definition of U_1, U_2, U are unchanged, we must reinterpret the slopes of the linear features observed in measurements. For Supp. Fig. 1(a,b) the slopes $m_{jk}, m_{ik}; k \in \{1,2\}$ are given by:

$$m_{jk} = \frac{\Delta V_{Sk}}{\Delta V_{Pk}} = \frac{E_{Ck}C_{P1} + UC_{Pk,\bar{k}}}{2e^2 - (E_{Ck}C_{Sk} + UC_{Sk,\bar{k}})} \tag{15}$$

$$m_{ik} = \frac{\Delta V_{Sk}}{\Delta V_{Pk}} = -\frac{E_{Ck}C_{P1} + UC_{Pk,\bar{k}}}{E_{Ck}C_{Sk} + UC_{Sk,\bar{k}}} \tag{16}$$

where $\bar{k} = 1(2)$ if $k = 2(1)$. Additional measurements are needed to solve for all capacitances. The slope of the feature observed in Supp. Fig. 1(c,d) is:

$$n_k = \frac{\Delta V_{Pk}}{\Delta V_{P\bar{k}}} = -\frac{E_{Ck}C_{P\bar{k},k} + UC_{P\bar{k}}}{E_{Ck}C_{Pk} + UC_{Pk,\bar{k}}} \tag{17}$$

where $k = 1$ for (c) and $k = 2$ for (d). We can now solve for four of the capacitances. It may be shown that:

$$-n_k \frac{m_{jk} m_{ik}}{m_{ik} - m_{jk}} = \frac{X}{2} \frac{C_{P\bar{k},k}}{C_k} + \frac{X-1}{2} \frac{C_{P\bar{k}}}{C_m} \tag{18}$$

$$\frac{m_{jk} m_{ik}}{m_{ik} - m_{jk}} = \frac{X}{2} \frac{C_{Pk}}{C_k} + \frac{X-1}{2} \frac{C_{Pk,\bar{k}}}{C_m} \tag{19}$$

Equations (18) and (19) may be solved for C_{Pk} and $C_{Pk,\bar{k}}$, yielding $C_{P1} = 17.4$ aF, $C_{P1,2} = 1.37$ aF, $C_{P2} = 11.7$ aF, $C_{P2,1} = 1.92$ aF.

In Supp. Fig. 1(e,f), the slopes are given by:

$$p_k = \frac{\Delta V_{Pk}}{\Delta V_{SD\bar{k}}} = -\frac{E_{Ck} C_{S\bar{k},k} + U C_{S\bar{k}}}{E_{Ck} C_{Pk} + U C_{Pk,\bar{k}}} \tag{20}$$

It may be shown that:

$$-p_k \frac{m_{jk} m_{ik}}{m_{ik} - m_{jk}} = \frac{X}{2} \frac{C_{S\bar{k},k}}{C_k} + \frac{X-1}{2} \frac{C_{S\bar{k}}}{C_m} \tag{21}$$

$$-\frac{m_{jk}}{m_{ik} - m_{jk}} = \frac{X}{2} \frac{C_{Sk}}{C_k} + \frac{X-1}{2} \frac{C_{Sk,\bar{k}}}{C_m} \tag{22}$$

Solving the system of equations (21) and (22) yields $C_{S1} = 60.3$ aF, $C_{S2} = 53.0$ aF, $C_{S1,2} = 7.19$ aF, and $C_{S2,1} = 13.1$ aF. We emphasize that capacitances like $C_{S2,1}$ are bigger than or comparable to C_m, and cannot be neglected.

The capacitances are summarized in Supp. Table I. By accounting for all of these capacitances, one can take measurements in such a way as to apply a source-drain bias without gating the dot (changing the effective dot levels), and have independent effective gates for each dot, as done in the manuscript and described in the supplementary information of previous work [2].

	Value (aF)
C_1	134
C_2	107
C_m	8.97
C_{P1}	17.4
C_{P2}	11.7
$C_{P1,2}$	1.37
$C_{P2,1}$	1.92
C_{S1}	60.3
C_{S2}	53.0
$C_{S1,2}$	7.19
$C_{S2,1}$	13.1

TABLE I. Experimentally derived capacitances.

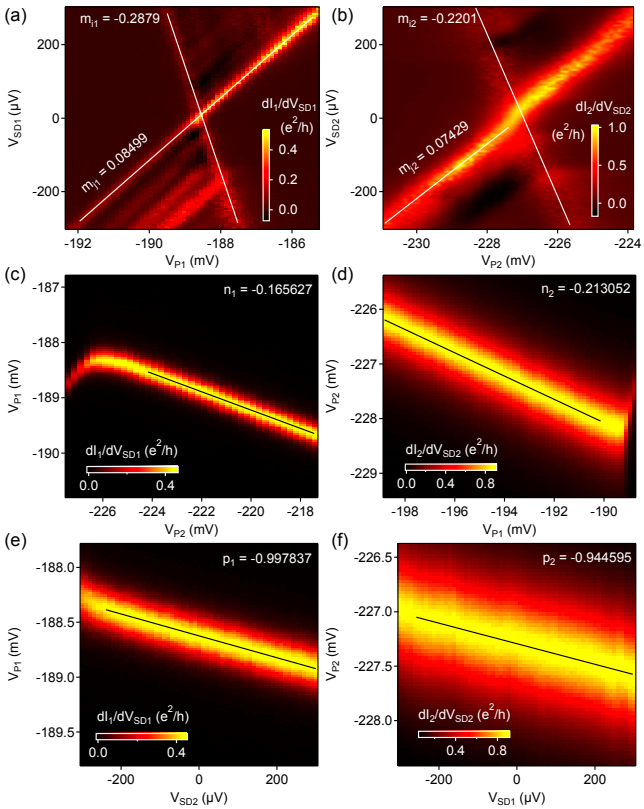

Supplementary Figure 1. Determining capacitances. (a) Source-drain bias spectroscopy for dot 1. $V_{P2} = -232.4$ mV is chosen to be away from the triple points. Slopes m_{i1}, m_{j1} are indicated. (b) Source-drain bias spectroscopy for dot 2. $V_{P1} = -193.8$ mV is chosen to be away from the triple points. Slopes m_{i2}, m_{j2} are indicated. (c,d) The capacitance of gate P2 to dot 1 (c) and gate P1 to dot 2 (d) may be obtained with these zero source-drain bias measurements. Slopes n_1, n_2 are indicated. (e,f) The capacitance of reservoir S2 to dot 1 (e) and S1 to dot 2 (f) may be obtained. Slopes p_1, p_2 are indicated. (e) $V_{P2} = -232.4$ mV. (f) $V_{P1} = -193.8$ mV.

B. LIMITS ON INTERDOT TUNNELING

The series conductance G_{series} at a triple point of the DQD places a limit on the interdot tunneling energy scale t. The series conductance is measured by applying an ac+dc bias voltage to both leads of dot 1 and using one current amplifier attached to both leads of dot 2 to measure current. In the case of zero dc bias [2, supp. info]:

$$G_{\text{series}} = \frac{64|t|^2}{3\Gamma_1\left(\frac{\Gamma_1+\Gamma_2}{2}\right)}\frac{e^2}{h} \tag{23}$$

where Γ_i is the total tunnel rate between dot i and its two leads S, i and D, i. In Supp. Fig. 2(a) we present conductance in a region of gate voltage containing the triple points of the DQD. For simplicity, here we are just varying the gate voltages $V_{P1,P2}$, rather than independently controlling $\varepsilon_{1,2}$. We switch measurement configurations in Supp. Fig. 2(b) and measure G_{series} at several dc biases, including zero bias. In contrast with transport through the individual dots (Supp. Fig. 2(a)), conductance through the two dots is at our noise floor. Perhaps a very faint signal can be observed for certain gate voltages at $V_{SD} = -200$ μV, but even there, $G_{\text{series}} < 2 \times 10^{-3}$ e^2/h for all measured dc biases. Given that $\Gamma_1 \sim 15$ μeV and $\Gamma_2 \sim 47$ μeV, we find that $|t| < 0.21$ μeV at zero dc bias. We do not rule out a dependence of $|t|$ on the bias voltage, but at least we do not observe appreciable G_{series} at non-zero bias either. To rule out the possibility that the triple points have drifted out of the measurement window owing to charge instability in the device, we immediately repeat the measurement of (a) in Supp. Fig. 2(c), and see that the features have barely moved.

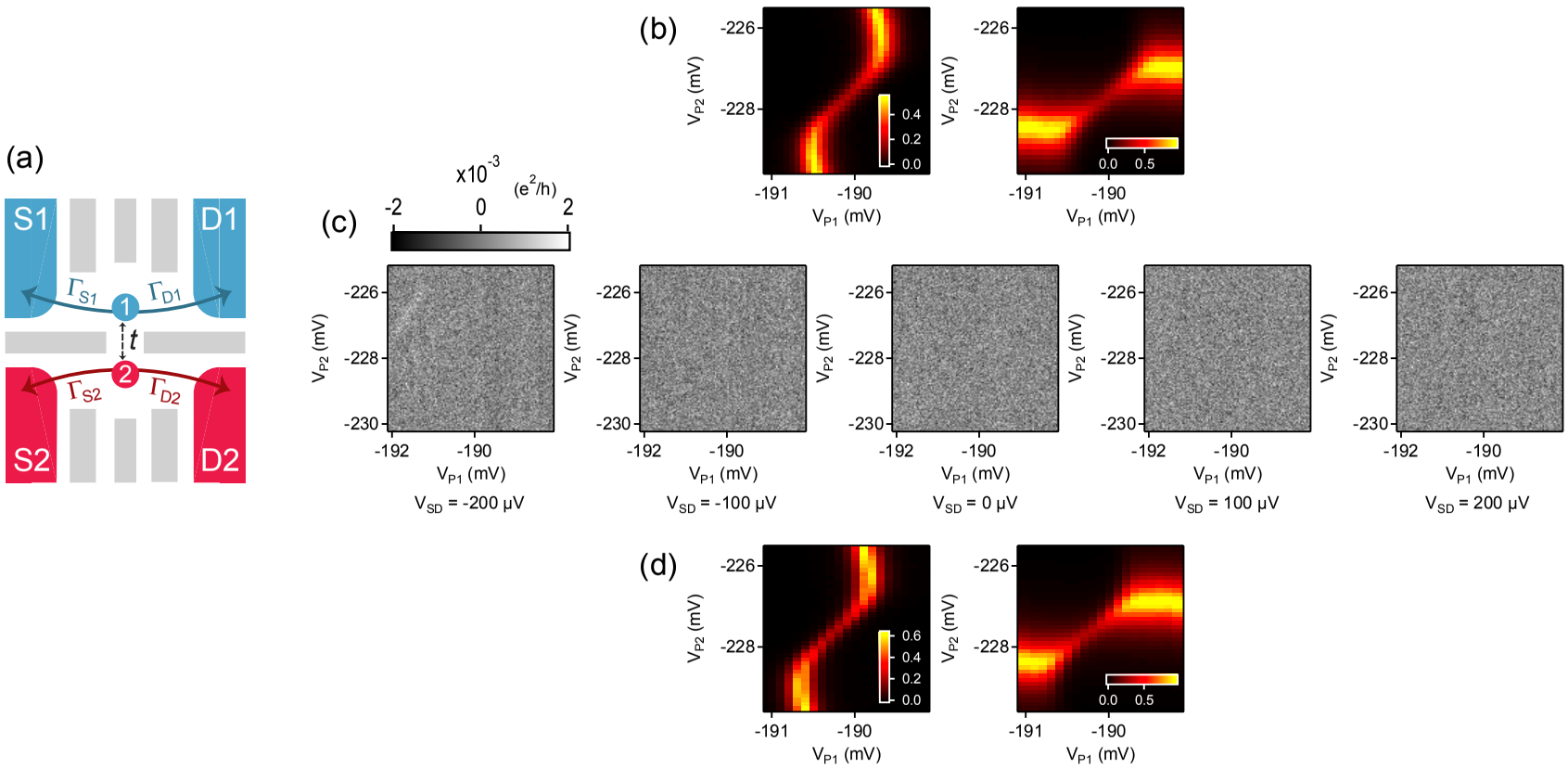

Supplementary Figure 2. Limits on interdot tunneling. (a) Interdot tunneling refers to direct hopping from dot 1 to dot 2 or vice versa. (b) Measured dI_1/dV_{S1} (left) and dI_2/dV_{S2} (right) at zero dc bias near triple points of the DQD. (c) Measured $G_{\text{series}} = dI/dV_{SD}$. The bias voltage is applied to both leads of dot 1 and current is measured by one current amplifier connected to both leads of dot 2. Five different dc biases were applied as indicated. No features are observed, except perhaps a faint signal when $V_{SD} = -200$ μV near the upper left of the plot. (d) Immediately after the measurements of (c), we repeat the measurements of (b) at lower resolution just to ensure that the features have not drifted. dI_1/dV_{S1} is again at left.

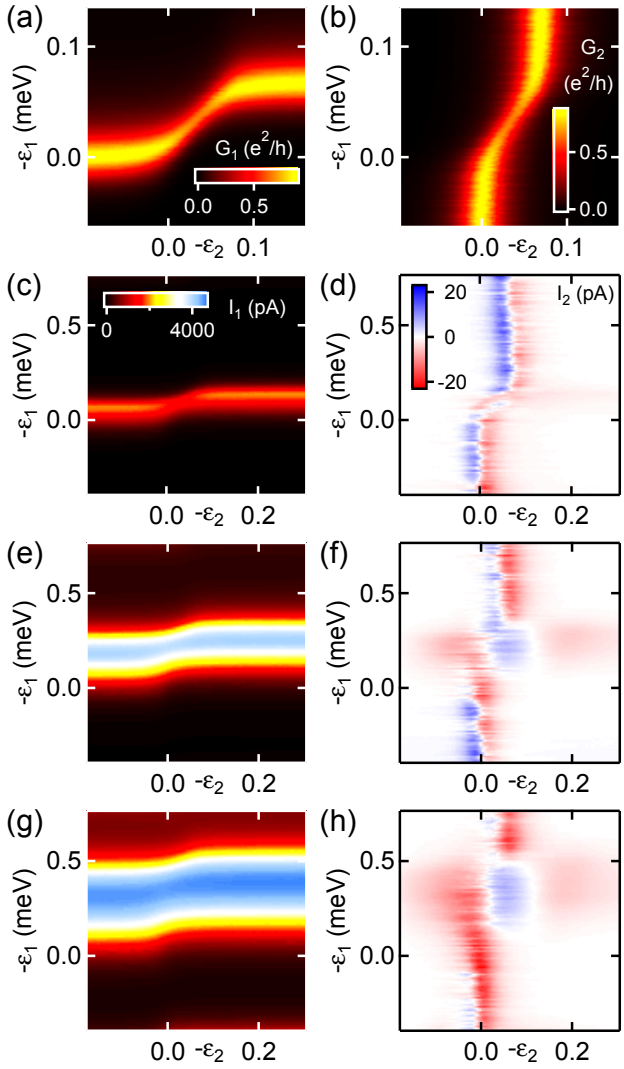

Supplementary Figure 3. Measurements with zero applied magnetic field. (a) Measured dI_1/dV_{SD1} and (b) dI_2/dV_{SD2} at zero dc bias near triple points of the DQD. (c,e,g) Measured I_1 and (d,f,h) I_2 for: (c,d) $V_{SD1} = 100$ μV; (e,f) $V_{SD1} = 300$ μV; (g,h) $V_{SD1} = 500$ μV. Note that in (c–h) the axis scaling differs from (a,b). No bias is applied across dot 2. In all cases, a drag current can be observed through dot 2 despite no explicit bias being applied to dot 2.

C. DRAG AT ZERO FIELD

Figures 2–4 show measurements taken in a large Zeeman field and small out-of-plane field. This is a regime where our (spinless) theory applies, and is where we took most drag measurements. For reference, Supplementary Figure 3 shows measurements taken in zero applied field. Qualitatively similar features are observed, including a finite drag current I_2 many linewidths away from resonance. A notable difference compared to the finite Zeeman field case is that the sign of I_2 changes as a function of $-\varepsilon_2$. This should not be surprising: even in the spinless theory we find that depending on tunnel couplings the direction of drag current can reverse in this way. This is true for both our model and the model in [3] (see their Fig. 3b).

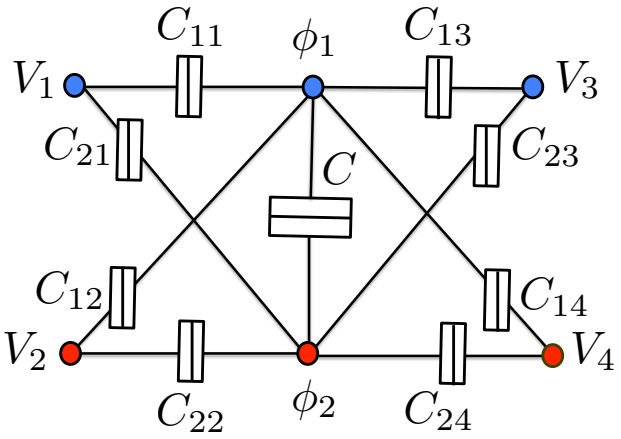

Supplementary Figure 4. Sketch of the electrostatic model.

D. THEORETICAL FORMALISM

1. Electrostatic model

We consider two capacitively coupled quantum dots, 1 and 2. With the geometry shown in Supp. Fig. 4, the electrostatic equations for the charges Q_1 and Q_2 are given by

$$Q_1 = \sum_i C_{1i}(\phi_1 - V_i) + C(\phi_1 - \phi_2)\,, \tag{24}$$

$$Q_2 = \sum_i C_{2i}(\phi_2 - V_i) + C(\phi_2 - \phi_1)\,, \tag{25}$$

with ϕ_1 and ϕ_2 the internal potentials and V_i $(i = 1, \ldots, 4)$ the applied voltages. The potential energies for both dots with $Q_1 = eN_1$ and $Q_2 = eN_2$ excess electrons take the form

$$U_1(N_1, N_2) = \int_0^{eN_1} \phi_1(Q_1, Q_2) dQ_1\,, \tag{26}$$

$$U_2(N_1, N_2) = \int_0^{eN_2} \phi_2(Q_1, Q_2) dQ_2\,, \tag{27}$$

where ϕ_1 and ϕ_2 are determined from Eqs. (24) and (25). The electrochemical potential of dots 1 and 2 can thus be written as

$$\mu_1 = \varepsilon_1 + U_1(1,0) - U_1(0,0)\,, \tag{28}$$

$$\mu_2 = \varepsilon_2 + U_2(0,1) - U_d(0,0)\,. \tag{29}$$

We have lumped the gate dependence into the values of the dot levels ε_1 and ε_2.

Let $\mu_{li} = E_F + eV_i$ be the electrochemical potential of lead i and $K = \sum_i C_{1i} \sum_j C_{2j} + C \sum_{i,j} C_{ij}$. Since the Fermi

functions are evaluated at $\mu_{S1}-\mu_1$, etc. (see main text), the energies of interest become

$$\mu_1-\mu_{l1}=\varepsilon_1-E_F+\frac{e}{K}\left[\frac{e(C+\sum_i C_{2i})}{2}+\sum_i C_{2i}\sum_j C_{1j}V_{j1}+C\sum_{i,j}C_{ij}V_{j1}\right], \tag{30a}$$

$$\mu_1-\mu_{l3}=\varepsilon_1-E_F+\frac{e}{K}\left[\frac{e(C+\sum_i C_{2i})}{2}+\sum_i C_{2i}\sum_j C_{1j}V_{j3}+C\sum_{i,j}C_{ij}V_{j3}\right], \tag{30b}$$

$$\mu_2-\mu_{l2}=\varepsilon_2-E_F+\frac{e}{K}\left[\frac{e(C+\sum_i C_{1i})}{2}+\sum_i C_{1i}\sum_j C_{2j}V_{j2}+C\sum_{i,j}C_{ij}V_{j2}\right], \tag{30c}$$

$$\mu_2-\mu_{l4}=\varepsilon_2-E_F+\frac{e}{K}\left[\frac{e(C+\sum_i C_{1i})}{2}+\sum_i C_{1i}\sum_j C_{2j}V_{j4}+C\sum_{i,j}C_{ij}V_{j4}\right], \tag{30d}$$

with $V_{ij}=V_i-V_j$. It is worth noting that these expressions depend on voltage differences only. Thus, our current expression will be gauge invariant.

When one of the dots is occupied, the electrochemical potentials can be evaluated as follows,

$$\mu_1=\varepsilon_1+\varepsilon_2+U_1(1,1)+U_2(1,1)-[\varepsilon_2+U_1(0,1)+U_2(0,1)], \tag{31}$$

$$\mu_2=\varepsilon_1+\varepsilon_2+U_1(1,1)+U_2(1,1)-[\varepsilon_1+U_1(1,0)+U_2(1,0)]. \tag{32}$$

Hence, Eq. (30) becomes

$$\mu_1-\mu_{l1}=\varepsilon_1-E_F+\frac{e}{K}\left[\frac{5e(C+\sum_i C_{2i})}{2}+\sum_i C_{2i}\sum_j C_{1j}V_{j1}+C\sum_{i,j}C_{ij}V_{j1}\right], \tag{33a}$$

$$\mu_1-\mu_{l3}=\varepsilon_1-E_F+\frac{e}{K}\left[\frac{5e(C+\sum_i C_{2i})}{2}+\sum_i C_{2i}\sum_j C_{1j}V_{j3}+C\sum_{i,j}C_{ij}V_{j3}\right], \tag{33b}$$

$$\mu_2-\mu_{l2}=\varepsilon_2-E_F+\frac{e}{K}\left[\frac{5e(C+\sum_i C_{1i})}{2}+\sum_i C_{1i}\sum_j C_{2j}V_{j2}+C\sum_{i,j}C_{ij}V_{j2}\right], \tag{33c}$$

$$\mu_2-\mu_{l4}=\varepsilon_2-E_F+\frac{e}{K}\left[\frac{5e(C+\sum_i C_{1i})}{2}+\sum_i C_{1i}\sum_j C_{2j}V_{j4}+C\sum_{i,j}C_{ij}V_{j4}\right]. \tag{33d}$$

Substracting Eq. (30) from Eq. (33), we find that the interdot Coulomb interaction corresponds to

$$U=\frac{2e^2C}{K}. \tag{34}$$

In our numerical calculations, we use the experimental parameters reported above: $C_{11}=C_{S1}$, $C_{12}=C_{S2,1}$, $C_{21}=C_{S1,2}$, $C_{22}=C_{S2}$, $C=C_m$ and $C_{13}=C_{23}=C_{14}=C_{24}=0$ together with $V_1=V_{S1}$, $V_2=V_{S2}$, $V_3=V_{D1}$ and $V_4=V_{D2}$.

2. Hamiltonian and tunnel rates

Our model Hamiltonian is

$$\mathcal{H}=\mathcal{H}_0+\mathcal{H}_T, \tag{35}$$

where

$$\mathcal{H}_0=\mathcal{H}_D+\mathcal{H}_C. \tag{36}$$

$\mathcal{H}_D$ is the Hamiltonian for the dot region,

$$\mathcal{H}_D = \sum_{i=1,2} \varepsilon_i d_i^\dagger d_i + U n_1 n_2 \,, \tag{37}$$

$\mathcal{H}_C$ corresponds to the reservoir Hamiltonian,

$$\mathcal{H}_C = \sum_{\alpha=S/D,i,k} \varepsilon_{\alpha k} c_{\alpha i k}^\dagger c_{\alpha i k} \,, \tag{38}$$

and finally $\mathcal{H}_T$ describes tunneling processes between the dot region and the reservoirs,

$$\mathcal{H}_T = \sum_{\alpha,i,k} \left(t_{\alpha i k} c_{\alpha i k}^\dagger d_i + h.c. \right) . \tag{39}$$

We regard $\mathcal{H}_T$ as a perturbation and calculate the probabilities for transitions between initial $|\psi_i\rangle$ and final $|\psi_f\rangle$ states (energies E_i and E_f, respectively) from an expansion of the T-matrix,

$$P_{if} = \frac{2\pi}{\hbar} \left| \langle \psi_f | \mathcal{H}_T + \mathcal{H}_T \mathcal{G}_0 \mathcal{H}_T + \cdots | \psi_i \rangle \right|^2 \delta(E_i - E_f) \,, \tag{40}$$

where the resolvent operator is $\mathcal{G}_0 = (E_i - \mathcal{H}_0)^{-1}$. To lowest order in $\mathcal{H}_T$ (Fermi's golden rule) one obtains sequential-tunneling transition rates between the dot states $|0\rangle = |00\rangle$, $|1\rangle = |10\rangle$, $|2\rangle = |01\rangle$ and $|d\rangle = |11\rangle$:

$$\Gamma_{0i}^{\alpha i} = \frac{1}{\hbar} \Gamma_{\alpha i} f_{\alpha i}(\mu_i) \,, \tag{41}$$

$$\Gamma_{0i}^{\alpha i} = \frac{1}{\hbar} \Gamma_{\alpha i} [1 - f_{\alpha i}(\mu_i)] \,, \tag{42}$$

$$\Gamma_{id}^{\alpha \bar{i}} = \frac{1}{\hbar} \gamma_{\alpha \bar{i}} f_{\alpha \bar{i}}(\mu_{\bar{i}} + U) \,, \tag{43}$$

$$\Gamma_{di}^{\alpha \bar{i}} = \frac{1}{\hbar} \gamma_{\alpha \bar{i}} \left[1 - f_{\alpha \bar{i}}(\mu_{\bar{i}} + U) \right] , \tag{44}$$

with $\Gamma_{\alpha i} = 2\pi \rho_{\alpha i} |t_{\alpha i}^0|^2$ and $\gamma_{\alpha i} = 2\pi \rho_{\alpha i} |t_{\alpha i}^1|^2$. As discussed in the main article, the transmission probabilities depend on energy and $t_{\alpha i}$ thus becomes a function of the charge state. In our numerical simulations of the drag current, we use the experimental values $2\Gamma_{S1} = 2\Gamma_{D1} = \Gamma_1 = 15$ μeV and $2\Gamma_{S2} = 2\Gamma_{D2} = \Gamma_2 = 47$ μeV and choose $\gamma_{S1} = \gamma_{D1} = \Gamma_{S1}$, $\gamma_{S2} = 0.5\Gamma_{S2}$ and $\gamma_{D2} = \Gamma_{D2}$.

To second order in $\mathcal{H}_T$ we obtain cotunneling transition rates involving many intermediate states which must be summed over:

$$\gamma_{if} = \frac{2\pi}{\hbar} \operatorname{Tr} W_i \left| \langle \psi_f | \mathcal{H}_T \frac{1}{E_i - \mathcal{H}_0} \mathcal{H}_T | \psi_i \rangle \right|^2 \delta(E_i - E_f) \,, \tag{45}$$

where the trace is performed over the lead degrees of freedom and the thermal factor W_i obeys

$$\sum_i W_i \left| \langle \psi_i | c_{\alpha k}^\dagger c_{\alpha k} | \psi_i \rangle \right| = f_\alpha(\varepsilon_{\alpha k}) \,. \tag{46}$$

In the following, we focus on the nondiagonal cotunneling rates since the terms γ_{00}, γ_{11}, γ_{22} and γ_{dd} do not contribute to the master equations (see below) or to the drag current:

$$\gamma_{i\bar{i}}^{\alpha\bar{i}\beta i} = \frac{2\pi}{\hbar} \int d\varepsilon \left| \frac{t_{\alpha\bar{i}}^0 t_{\beta i}^0}{\varepsilon - \mu_{\bar{i}} + i\eta} - \frac{t_{\alpha\bar{i}}^1 t_{\beta i}^1}{\varepsilon - \mu_{\bar{i}} - U + i\eta} \right|^2 \rho_{\alpha\bar{i}} \rho_{\beta i} f_{\alpha\bar{i}}(\varepsilon) \left[1 - f_{\beta i}(\varepsilon + \mu_i - \mu_{\bar{i}}) \right] , \tag{47a}$$

$$\gamma_{0d}^{\alpha\bar{i}\beta i} = \frac{2\pi}{\hbar} \int d\varepsilon \left| \frac{t_{\alpha\bar{i}}^0 t_{\beta i}^1}{\varepsilon - \mu_{\bar{i}} + i\eta} - \frac{t_{\alpha\bar{i}}^1 t_{\beta i}^0}{\varepsilon - \mu_{\bar{i}} - U + i\eta} \right|^2 \rho_{\alpha\bar{i}} \rho_{\beta i} f_{\alpha\bar{i}}(\varepsilon) f_{\beta i}(\mu_i + \mu_{\bar{i}} + U - \varepsilon) \,, \tag{47b}$$

$$\gamma_{d0}^{\alpha\bar{i}\beta i} = \frac{2\pi}{\hbar} \int d\varepsilon \left| \frac{t_{\alpha\bar{i}}^0 t_{\beta i}^1}{\varepsilon - \mu_{\bar{i}} + i\eta} - \frac{t_{\alpha\bar{i}}^1 t_{\beta i}^0}{\varepsilon - \mu_{\bar{i}} - U + i\eta} \right|^2 \rho_{\alpha\bar{i}} \rho_{\beta i} \left[1 - f_{\alpha\bar{i}}(\varepsilon) \right] \left[1 - f_{\beta i}(\mu_i + \mu_{\bar{i}} + U - \varepsilon) \right] , \tag{47c}$$

where a finite broadening η (a small imaginary part) has been added to the denominators in order to avoid the divergence associated to the infinite lifetime of the intermediate states. Expansion in powers of $1/\eta$ leads to a first term which reproduces the sequential tunneling result. Therefore, to avoid double counting we subtract this term. The next order is independent of η and corresponds to the nondivergent cotunneling expressions. We find

$$\begin{aligned}\gamma_{i\bar{i}}^{\alpha\bar{i}\beta i} &= \frac{\beta}{4\pi^2\hbar}\Gamma_{\alpha\bar{i}}\Gamma_{\beta i} n_B(\mu_{\bar{i}}-\mu_i+\mu_{\beta i}-\mu_{\alpha\bar{i}})\,\mathrm{Im}\left\{\Psi^{(1)}\left(\frac{1}{2}+i\beta\frac{\mu_{\bar{i}}-\mu_{\alpha\bar{i}}}{2\pi}\right)-\Psi^{(1)}\left(\frac{1}{2}+i\beta\frac{\mu_i-\mu_{\beta i}}{2\pi}\right)\right\}\\ &+\frac{\beta}{4\pi^2\hbar}\gamma_{\alpha\bar{i}}\gamma_{\beta i} n_B(\mu_{\bar{i}}-\mu_i+\mu_{\beta i}-\mu_{\alpha\bar{i}})\,\mathrm{Im}\left\{\Psi^{(1)}\left(\frac{1}{2}+i\beta\frac{\mu_{\bar{i}}+U-\mu_{\alpha\bar{i}}}{2\pi}\right)-\Psi^{(1)}\left(\frac{1}{2}+i\beta\frac{\mu_i+U-\mu_{\beta i}}{2\pi}\right)\right\}\\ &-\frac{\sqrt{\Gamma_{\alpha\bar{i}}\Gamma_{\beta i}\gamma_{\alpha\bar{i}}\gamma_{\beta i}}}{\pi\hbar} n_B(\mu_{\bar{i}}-\mu_i+\mu_{\beta i}-\mu_{\alpha\bar{i}})\frac{1}{U}\,\mathrm{Re}\left\{\Psi\left(\frac{1}{2}+i\beta\frac{\mu_{\bar{i}}-\mu_{\alpha\bar{i}}}{2\pi}\right)-\Psi\left(\frac{1}{2}-i\beta\frac{\mu_{\bar{i}}+U-\mu_{\alpha\bar{i}}}{2\pi}\right)\right.\\ &\left.-\Psi\left(\frac{1}{2}+i\beta\frac{\mu_i-\mu_{\beta i}}{2\pi}\right)+\Psi\left(\frac{1}{2}-i\beta\frac{\mu_i+U-\mu_{\beta i}}{2\pi}\right)\right\}, \qquad (48a)\end{aligned}$$

$$\begin{aligned}\gamma_{0d}^{\alpha\bar{i}\beta i} &= \frac{\beta}{4\pi^2\hbar}\Gamma_{\alpha\bar{i}}\gamma_{\beta i} n_B(\mu_i+\mu_{\bar{i}}+U-\mu_{\alpha\bar{i}}-\mu_{\beta i})\,\mathrm{Im}\left\{\Psi^{(1)}\left(\frac{1}{2}+i\beta\frac{\mu_{\bar{i}}-\mu_{\alpha\bar{i}}}{2\pi}\right)+\Psi^{(1)}\left(\frac{1}{2}+i\beta\frac{\mu_i+U-\mu_{\beta i}}{2\pi}\right)\right\}\\ &+\frac{\beta}{4\pi^2\hbar}\gamma_{\alpha\bar{i}}\Gamma_{\beta i} n_B(\mu_i+\mu_{\bar{i}}+U-\mu_{\alpha\bar{i}}-\mu_{\beta i})\,\mathrm{Im}\left\{\Psi^{(1)}\left(\frac{1}{2}+i\beta\frac{\mu_{\bar{i}}+U-\mu_{\alpha\bar{i}}}{2\pi}\right)+\Psi^{(1)}\left(\frac{1}{2}+i\beta\frac{\mu_i-\mu_{\beta i}}{2\pi}\right)\right\}\\ &-\frac{\sqrt{\Gamma_{\alpha\bar{i}}\Gamma_{\beta i}\gamma_{\alpha\bar{i}}\gamma_{\beta i}}}{\pi\hbar} n_B(\mu_i+\mu_{\bar{i}}+U-\mu_{\alpha\bar{i}}-\mu_{\beta i})\frac{1}{U}\,\mathrm{Re}\left\{\Psi\left(\frac{1}{2}+i\beta\frac{\mu_{\bar{i}}-\mu_{\alpha\bar{i}}}{2\pi}\right)-\Psi\left(\frac{1}{2}-i\beta\frac{\mu_{\bar{i}}+U-\mu_{\alpha\bar{i}}}{2\pi}\right)\right.\\ &\left.+\Psi\left(\frac{1}{2}+i\beta\frac{\mu_i-\mu_{\beta i}}{2\pi}\right)-\Psi\left(\frac{1}{2}-i\beta\frac{\mu_i+U-\mu_{\beta i}}{2\pi}\right)\right\}, \qquad (48b)\end{aligned}$$

$$\begin{aligned}\gamma_{d0}^{\alpha\bar{i}\beta i} &= \frac{\beta}{4\pi^2\hbar}\Gamma_{\alpha\bar{i}}\gamma_{\beta i}\left[1+n_B(\mu_i+\mu_{\bar{i}}+U-\mu_{\alpha\bar{i}}-\mu_{\beta i})\right]\mathrm{Im}\left\{\Psi^{(1)}\left(\frac{1}{2}+i\beta\frac{\mu_{\bar{i}}-\mu_{\alpha\bar{i}}}{2\pi}\right)+\Psi^{(1)}\left(\frac{1}{2}+i\beta\frac{\mu_i+U-\mu_{\beta i}}{2\pi}\right)\right\}\\ &+\frac{\beta}{4\pi^2\hbar}\gamma_{\alpha\bar{i}}\Gamma_{\beta i}\left[1+n_B(\mu_i+\mu_{\bar{i}}+U-\mu_{\alpha\bar{i}}-\mu_{\beta i})\right]\mathrm{Im}\left\{\Psi^{(1)}\left(\frac{1}{2}+i\beta\frac{\mu_{\bar{i}}+U-\mu_{\alpha\bar{i}}}{2\pi}\right)+\Psi^{(1)}\left(\frac{1}{2}+i\beta\frac{\mu_i-\mu_{\beta i}}{2\pi}\right)\right\}\\ &-\frac{\sqrt{\Gamma_{\alpha\bar{i}}\Gamma_{\beta i}\gamma_{\alpha\bar{i}}\gamma_{\beta i}}}{\pi\hbar}\left[1+n_B(\mu_i+\mu_{\bar{i}}+U-\mu_{\alpha\bar{i}}-\mu_{\beta i})\right]\frac{1}{U}\,\mathrm{Re}\left\{\Psi\left(\frac{1}{2}+i\beta\frac{\mu_{\bar{i}}-\mu_{\alpha\bar{i}}}{2\pi}\right)-\Psi\left(\frac{1}{2}-i\beta\frac{\mu_{\bar{i}}+U-\mu_{\alpha\bar{i}}}{2\pi}\right)\right.\\ &\left.+\Psi\left(\frac{1}{2}+i\beta\frac{\mu_i-\mu_{\beta i}}{2\pi}\right)-\Psi\left(\frac{1}{2}-i\beta\frac{\mu_i+U-\mu_{\beta i}}{2\pi}\right)\right\}. \qquad (48c)\end{aligned}$$

Here, $n_B(x) = 1/(e^x-1)$ is the Bose distribution function, Ψ ($\Psi^{(1)}$) is the digamma (trigamma) function and $\beta = 1/k_BT$ is the inverse temperature.

The stationary values of the set of probabilities $\boldsymbol{p} = (p_0, p_1, p_2, p_d)^T$ follow from the equations $0 = \boldsymbol{\Gamma p}$ written in matrix form with

$$\boldsymbol{\Gamma} = \begin{pmatrix} -(\Gamma_{01}+\Gamma_{02}+\gamma_{0d}) & \Gamma_{10} & \Gamma_{20} & \gamma_{d0} \\ \Gamma_{01} & -(\Gamma_{10}+\Gamma_{1d}+\gamma_{12}) & \gamma_{21} & \Gamma_{d1} \\ \Gamma_{02} & \gamma_{12} & -(\Gamma_{20}+\Gamma_{2d}+\gamma_{21}) & \Gamma_{d2} \\ \gamma_{0d} & \Gamma_{1d} & \Gamma_{2d} & -(\Gamma_{d1}+\Gamma_{d2}+\gamma_{d0}) \end{pmatrix}, \qquad (49)$$

where

$$\begin{aligned}&\Gamma_{01}=\sum_\alpha \Gamma_{01}^{\alpha 1}, \quad \Gamma_{10}=\sum_\alpha \Gamma_{10}^{\alpha 1}, \quad \Gamma_{02}=\sum_\alpha \Gamma_{02}^{\alpha 2}, \quad \Gamma_{20}=\sum_\alpha \Gamma_{20}^{\alpha 2},\\ &\Gamma_{1d}=\sum_\alpha \Gamma_{1d}^{\alpha 2}, \quad \Gamma_{d1}=\sum_\alpha \Gamma_{d1}^{\alpha 2}, \quad \Gamma_{2d}=\sum_\alpha \Gamma_{2d}^{\alpha 1}, \quad \Gamma_{d2}=\sum_\alpha \Gamma_{d2}^{\alpha 1},\\ &\gamma_{12}=\sum_{\alpha,\beta} \gamma_{12}^{\alpha 2\beta 1}, \quad \gamma_{21}=\sum_{\alpha,\beta} \gamma_{21}^{\alpha 1\beta 2}, \quad \gamma_{0d}=\sum_{\alpha,\beta} \gamma_{0d}^{\alpha 1\beta 2}, \quad \gamma_{d0}=\sum_{\alpha,\beta} \gamma_{d0}^{\alpha 1\beta 2},\end{aligned} \qquad (50a)$$

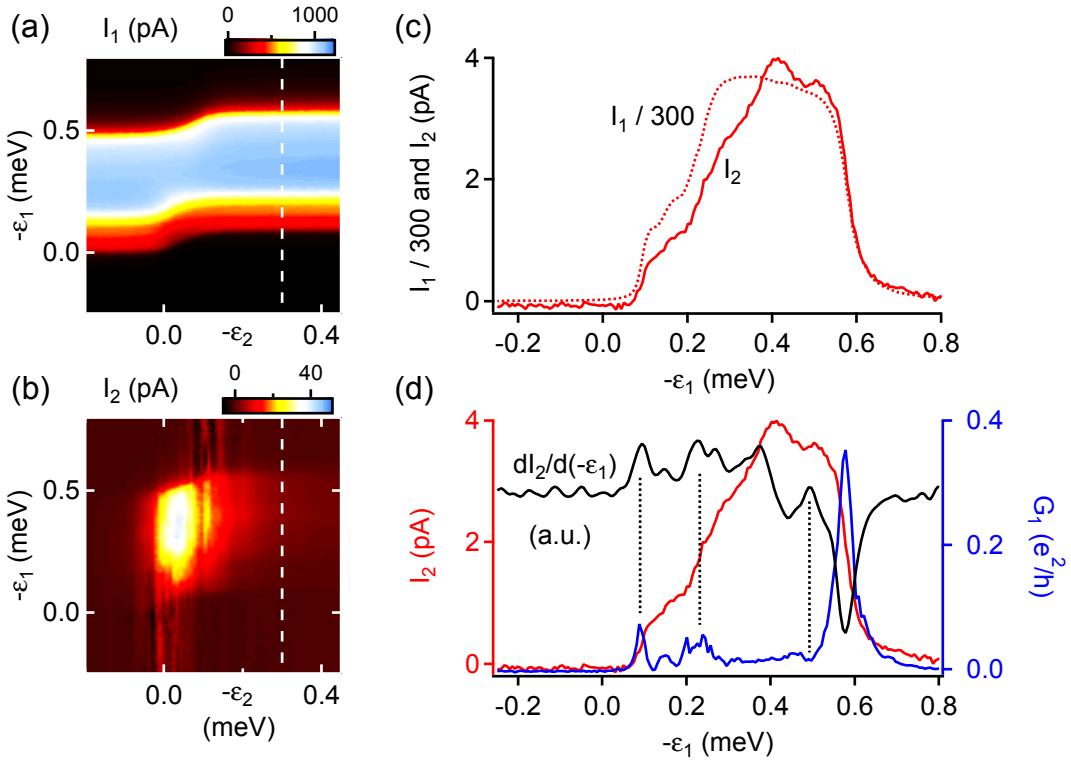

Supplementary Figure 5. Extended data and analysis from Fig. 2 ($V_{S1} = 0.5$ mV, $V_{S2} = 0$; $-\varepsilon_2 = 0.3$ meV where cuts are shown). (a) Drive current I_1. (b) Drag current I_2. This is a reproduction of Fig. 2(e) to aid in comparing with Supp. Fig. 5(a). (c) Cuts from Supp. Fig. 5(a) and Supp. Fig. 5(b). I_1 has been divided by 300 to fit on the same scale. (d) Numerically differentiated $dI_2/d(-\epsilon_1)$ (black, arbitrary units) is correlated, positively or negatively, with G_1 (blue, right axis). G_1 has been taken from the cut in Fig. 2(c) and I_2 is the same trace as above in Supp. Fig. 5(c). The correlated features appear generic in region (iii) as defined in Fig. 2(a).

E. EXTENDED DATA AND ANALYSIS FROM FIG. 2

In Supp. Fig. 5(a) we show the drive current I_1 as a function of $-\varepsilon_1$ and $-\varepsilon_2$ for the same parameters as used in Fig. 2. For ease of comparison, Supp. Fig. 5(b) reproduces Fig. 2(e), the drag current I_2. Supplementary Figure 5(c) compares I_1 and I_2 for $-\varepsilon_2 = 0.3$ meV. The drag current is seen to be less than a percent of the drive current, which is typical for region (iii), although the ratio can reach a few percent in region (ii).

In Supp. Fig. 5d we compare the vertical cuts in Fig. 2(c) and 2(e). Peaks and dips in G_1 are correlated (or anticorrelated) with peaks and dips in numerically calculated $dI_2/d(-\varepsilon_1)$. There appears to be correlation near $-\varepsilon_1 = U = 0.1$ meV, and anticorrelation nearer to $-\varepsilon_1 = U + |e|V_{S1} = 0.6$ meV. In the middle, G_1 is flat and there appears to be no correlation. As the peaks in G_1 correspond to excited states in dot 1, these features may not be explained satisfactorily by existing theories, and are well-resolved in the low temperature regime.

* Present address: Institute for Quantum Information and Matter, California Institute of Technology, Pasadena, California 91125, USA
† Present address: MIT Lincoln Laboratory, Lexington, Massachusetts 02420, USA
‡ goldhaber-gordon@stanford.edu

[1] W. G. Van der Wiel, S. De Franceschi, J. M. Elzerman, T. Fujisawa, S. Tarucha, and L. P. Kouwenhoven, Rev. Mod. Phys. **75**, 1 (2002).
[2] S. Amasha, A. J. Keller, I. G. Rau, A. Carmi, J. A. Katine, H. Shtrikman, Y. Oreg, and D. Goldhaber-Gordon, Phys. Rev. Lett. **110**, 046604 (2013).
[3] K. Kaasbjerg and A.-P. Jauho, Phys. Rev. Lett. **116**, 196801 (2016).